Waveguide-integrated single- and multi-photon detection at telecom wavelengths using superconducting nanowires

Simone Ferrari; Oliver Kahl; Vadim Kovalyuk; ... et. al

Check for updates

CrossMark

View Online   Export Citation

Articles You May Be Interested In

Photon-number-resolving SSPDs with system detection efficiency over 50% at telecom range

AIP Conference Proceedings (February 2018)

Operating quantum waveguide circuits with superconducting single-photon detectors

Appl. Phys. Lett. (May 2010)

In-line silicon Schottky photodetectors on silicon cored fibers working in 1550 nm wavelength regimes

Appl. Phys. Lett. (May 2015)

Applied Physics Letters

AIP Publishing

Waveguide-integrated single- and multi-photon detection at telecom wavelengths using superconducting nanowires

Simone Ferrari,[1,a)] Oliver Kahl,[1,a)] Vadim Kovalyuk,[1,2,a)] Gregory N. Goltsman,[2,3] Alexander Korneev,[2,4] and Wolfram H. P. Pernice[1,5,b)]

[1]Institute of Nanotechnology, Karlsruhe Institute of Technology, Karlsruhe 76132, Germany
[2]Department of Physics, Moscow State Pedagogical University, Moscow 119992, Russia
[3]National Research University Higher School of Economics, 20 Myasnitskaya Ulitsa, Moscow 101000, Russia
[4]Moscow Institute of Physics and Technology (State University), Moscow 141700, Russia
[5]Department of Physics, University of Münster, 48149 Münster, Germany

We investigate single- and multi-photon detection regimes of superconducting nanowire detectors embedded in silicon nitride nanophotonic circuits. At near-infrared wavelengths, simultaneous detection of up to three photons is observed for 120 nm wide nanowires biased far from the critical current, while narrow nanowires below 100 nm provide efficient single photon detection. A theoretical model is proposed to determine the different detection regimes and to calculate the corresponding internal quantum efficiency. The predicted saturation of the internal quantum efficiency in the single photon regime agrees well with plateau behavior observed at high bias currents. © 2015 AIP Publishing LLC.
[http://dx.doi.org/10.1063/1.4917166]

For demanding applications in photon counting,[1] quantum optics,[2,3] as well as correlation imaging,[4] high efficiency single photon detectors with superior performance are required. Depending on the target optical wavelength, different detector implementations can be used. In the visible wavelength range, the current detector of choice is the silicon avalanche photodiode (APD).[5–7] Such detectors provide high timing resolution and detection efficiency above 70% at moderate dark count levels.[8,9] When moving to near-infrared wavelengths, indium gallium arsenide (InGaAs) based APDs can be employed.[7,10] InGaAs APDs suffer, however, from higher dark count rates, lower detection efficiency, and need to be operated in gated mode.[8–11] Alternatively, superconducting single-photon detectors (SSPDs) offer broad optical bandwidth, high detection efficiency, and high timing resolution in the same device.[12,13] SSPDs thus promise to overcome limitations of traditional single photon detectors particularly at telecommunication wavelengths.[14] For use in integrated quantum optical applications conventional free-space SSPDs[15] are nevertheless hard to combine with an on-chip framework. Instead, full scalability and integration atop of waveguides in optical circuits are desirable to provide essential elements for applications in quantum photonic technologies.[16–19] Here, we demonstrate that niobium nitride (NbN) nanowire SSPDs atop silicon nitride (Si₃N₄) nanophotonic waveguide not only provide single-photon counting capability but also can be used to discriminate larger numbers of photons when operated under different biasing conditions. We present a simple model to accurately fit our experimental data, which allows us to extract the internal quantum efficiency (IQE) of the integrated detectors. Our results allow for designing tailored integrated nanophotonic devices which operate in a desirable detection regime by selecting opportune biasing conditions.

The SSPDs in this work are fabricated from a 4 nm thick superconducting NbN film deposited by magnetron sputtering in argon/nitrogen atmosphere onto 450 nm thick stoichiometric Si₃N₄ films sitting on top of a SiO₂ layer on a Si substrate. Superconducting nanowire detector devices are realized with a three steps lithography process for integration with nanophotonic circuitry. In an initial e-beam exposure, metal contact pads and alignment marker patterns are defined using the positive resist polymethyl methacrylate (PMMA). Contact pads and markers are then finalized by electron beam evaporation of 150 nm gold on a 5 nm thick chromium adhesion layer and subsequent lift-off in acetone. Subsequently, the detector nanowires are defined by high resolution e-beam lithography using hydrogen silsesquioxane (HSQ). The pattern is transferred into the NbN layer using CF₄ plasma reactive ion etching (RIE). In the final exposure, nanophotonic waveguides are written with ma-N 2403 resist, followed by a second dry etching step using RIE with a CHF₃ chemistry to obtain an half etched rib-waveguide structures on Si₃N₄. An additional O₂ plasma step is used to remove the residual resist on the top of the waveguides. With this procedure low loss waveguides (21 dB/m) can be reliably fabricated.[20]

An SEM picture of a typical nanophotonic circuit is shown in the inset of Fig. 1(c). We use nanophotonic devices into which light is injected and collected from waveguides which support transverse-electrical (TE) mode propagation using an optical fiber array and a pair of optical grating couplers, designed for 1550 nm wavelength. The integrated optical circuit (Fig. 1(d)) consists of a 50:50 waveguide splitter that routes half of the coupled light to the detector region and the other half to a reference grating coupler port which is used to determine the amount of photons travelling to the detector. The SSPDs are fabricated directly on the top of the waveguide so that for sufficiently long nanowires the incoming photons are almost fully absorbed.[21] This design offers significant advantages in terms of the overall on–chip detection efficiency in comparison with traditional fiber coupled SSPDs,

---

a)S. Ferrari, O. Kahl, and V. Kovalyuk contributed equally to this work.
b)Author to whom correspondence should be addressed. Electronic mail: wolfram.pernice@kit.edu.
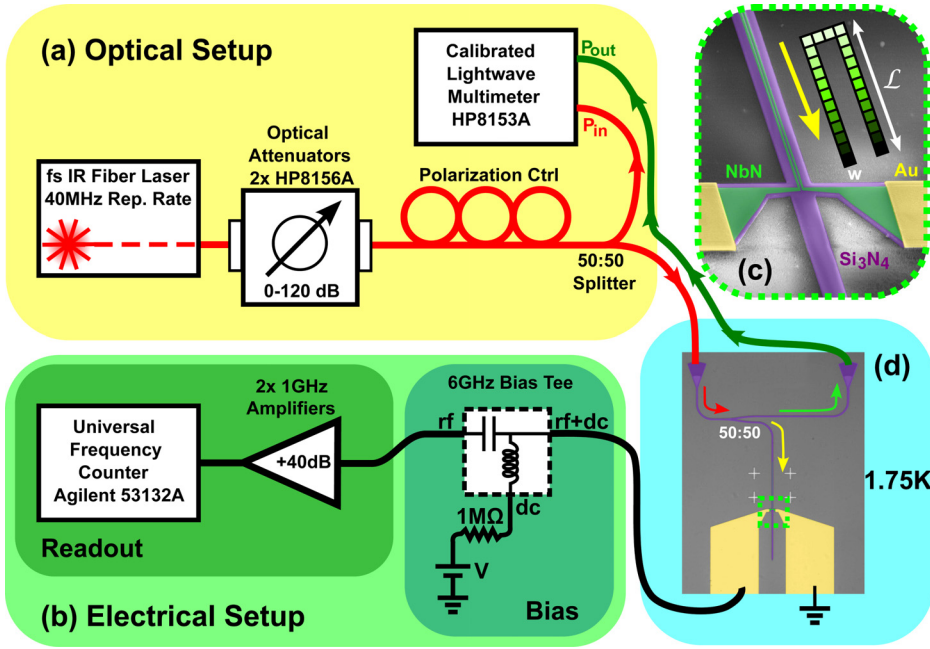
FIG. 1. Experimental setup for the detection probability measurement. (a) Optical setup: 1550 nm pulses from a femtosecond laser are injected into the optical circuit through a pair of attenuators and a polarization controller. The generated signal is divided by a 50:50 splitter and registered by a lightwave multimeter. (b) Electrical setup: the detectors are biased by a stable source (Keithley 2400) and the output signal is registered by a frequency counter after being amplified by low noise amplifiers (mini circuits ZFL-1000LN+). The inset (c) shows an SEM picture of the nanowire (green) atop the waveguide (purple) and the contact pads (gold) and a schematic of the nanowire mesh used for the theoretical model. (d) Optical micrograph of the on-chip optical circuit (purple) and the nanowire contact pads (gold).

which absorb photons only under normal incidence in an ultra-thin superconducting meander structure.[16,22]

The detection mechanism of nanowire SSPDs can be understood in the framework of the quasi-static vortex (QSV) model, combined with quasi-particle diffusion.[23–25] The absorption of a photon increases locally the temperature of electrons, thus forming a hot-spot inside the nanowire. Suppression of the order parameter in the spot and the corresponding enhancement of the kinetic inductivity lead to redistribution of the supercurrent density. If the suppression of the order parameter and supercurrent are sufficient, the supercurrent density exceeds the depairing current density in the center of the spot or at the edge of the strip, depending on whether the spot was formed near the center of the strip or near the edge. Immediately after this, a vortex-antivortex pair or a single vortex is nucleated and crosses the strip, that locally heats it up, leading to a further reduction of the depairing current density and also the nucleation of new vortices. Model calculations[24] show that for films with high resistivity, like NbN, crossing of the strip by just several vortices or pairs completely destroys the superconductivity in the narrow belt across the strip. The breakdown of the superconductivity corresponds to the appearance of resistance and thus a detection event. Then the supercurrent is reduced, heating stops and the superconducting state is recovered on a picosecond timescale through thermalization with the cold bath. If the value of the supercurrent is not sufficiently large or the width of the strip is too large, after the formation of the hot spot, the redistributed supercurrent density will not exceed the depairing current density, and the absorption of a single photon is insufficient to generate an output signal. Instead, the simultaneous absorption of multiple photons in a small region of the wire is needed to lead to a breakdown of the superconductivity. In addition, the multi-photon absorption events must occur within the original hotspot lifetime.

In order to measure multi-photon absorption, we employ the measurement setup shown in Fig. 1. A 1550 nm femtosecond laser (PriTel FFL-40M), with a repetition rate RR of 40.125 MHz, generates pulses that are sent through two optical attenuators (HP 8156A) which provide maximum attenuation of 120 dB. The attenuated pulses pass through a polarization controller to optimize the transmission through the optical circuit which is situated in a helium-4 flow cryostat with a base temperature of 1.75 K. The superconducting nanowire is biased in current mode by a stable voltage source (Keithley 2400) connected to a 1 MΩ series resistor and a bias tee (ZFBT-GW6+). The readout circuit consists of two low noise amplifiers (mini circuits ZFL-1000LN+) connected to a frequency counter (Agilent 53132A). In order to exactly control the average number of photons arriving at the on-chip detector, a lightwave multimeter system (HP 8135A) is used to continuously monitor the optical input power. A critical point in the exact determination of the number of photons reaching the device is represented by the variability of the coupling efficiency of the grating couplers. This contribution is strongly dependent on the relative position between the fiber array and grating couplers, and may also vary for different devices.[18] Therefore, the effective coupling losses of the grating couplers are retrieved during the experiment by comparing the transmitted optical signal from the reference port of the on-chip optical circuit P_{out} and the input power P_{in}.

We measure the SSPDs' detection probability (DP) as the ratio between the detector count rate and the pulsed laser repetition rate, in dependence of the average number of photons per pulse in the waveguide. The average number of photons per pulse m that reaches the detector is calculated considering the attenuated laser power P_{in}, the femtosecond laser pulse repetition rate RR, the grating coupler coupling losses CL, the splitting ratio $S = 0.5$ of the 50/50 Y-splitter, and the waveguide losses WL, as follows:

$$m = \frac{\lambda}{hc} \frac{P_{in}}{RR} \times CL \times S \times WL. \qquad (1)$$

The measured detection probability for a 120 nm wide nanowire detector at different bias currents is shown in Fig. 2(a). For high bias currents, the detection probability grows linearly with the number of incoming photons. By reducing
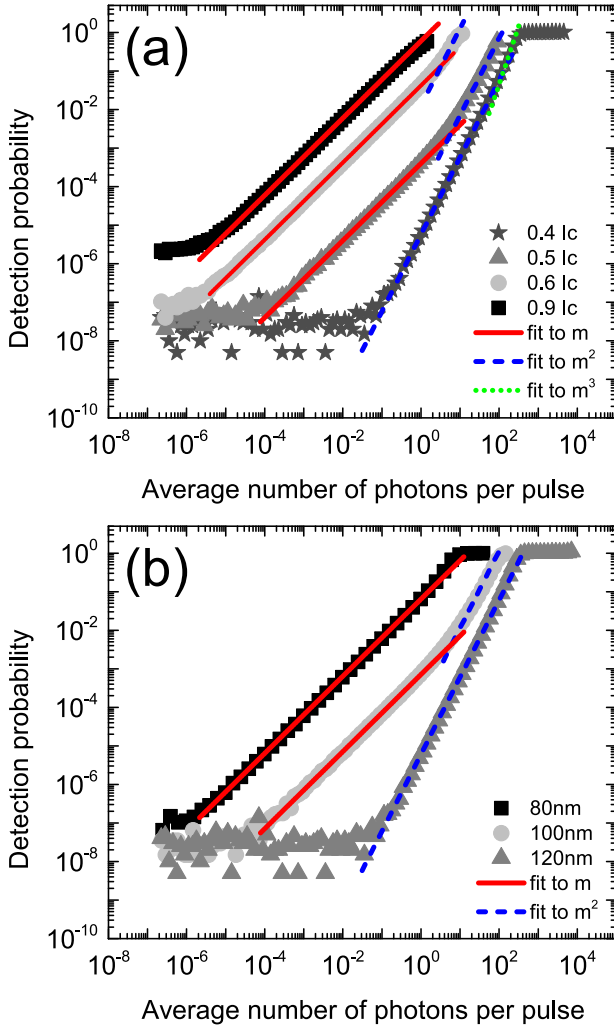
FIG. 2. (a) Measured detection probability vs average number of photons per pulse for a SSPD with a nanowire width of 120 nm at different bias currents. (b) Comparison of the detection probability measured for different nanowire widths at the same biasing condition (0.4 Ic). Indicated also is the fitted slope of the detection probability according to the model proposed by Elezov *et al.*[26]

the bias current, this proportionality becomes non-linear which on a log-log scale translates into a change of the slope of the detection curve. A similar behavior occurs when applying identical bias condition to detectors with different nanowire widths, as depicted in Fig. 2(b). The two data sets illustrate that for a large number of incoming photons the DP saturates, meaning that all the incoming pulses are detected. This saturation occurs at lower photon numbers for narrower wires and also at higher bias currents. For wider wires biased far away from the critical current, the absorption of a single photon is insufficient for breaking the superconductivity. Therefore, in order to produce a voltage signal, the absorption of multiple photons in the same region of the nanowire is needed. By investigating the different detection regimes, it is thus possible to arrive at suitable designs of the SSPDs which are capable of detecting the simultaneous arrival of a specific number n of photons rather than single photons. This property may be of particular interest for the detection of Fock or NOON states.

The total detection probability of fiber coupled SSPD can be described using the theoretical model proposed by Elezov *et al.*[26] Here, we adapted the formalism for the

waveguide integrated detector design, in which irradiation is not homogeneous along the wire. In a waveguide, the detection probability depends on two main contributions: the detector's *IQE* and the probability $\Psi^{(n)}$ of absorbing n photons at once

$$DP_{tot} = \sum_n IQE^{(n)} \Psi^{(n)}. \qquad (2)$$

The *IQE* corresponds to the probability of converting an absorbed photon into a detector output signal. This value is an intrinsic characteristic of the nanowire and depends on how the bias current is chosen with respect to the critical current for a given nanowire width. The *IQE* is typically limited by inhomogeneities in the nanowire width resulting from fabrication imperfections.[27] The second contribution $\Psi^{(n)}$ can be calculated by dividing each nanowire strip with a length $\mathcal{L}$, into a number of squares with edge length equal to the width w of the wire, as shown in the inset (c) of Fig. 1. Creating a device mesh this way agrees with the QSV model, since the final normal-conducting area has to span the entire nanowire width w in order to generate a detection signal.

We also have to consider that only one nanowire cell is able to provide a useful contribution for generating the voltage signal per detection cycle, especially for high optical input power. Therefore, the total absorption probability can be defined as the product of the probability of absorbing a photon in a strip cell $P_j^{(n)}$ and the probability of not absorbing photons in the other cells $\Xi_j^{(n)}$

$$\Psi^{(n)} = 2 \sum_{j=0}^{\mathcal{L}/w} P_j^{(n)} \Xi_j^{(n)}. \qquad (3)$$

The factor of 2 accounts for the fact that the detector consists of two parallel superconducting stripes. The marginal contribution originating from the 180° bend which connects the two stripes at one end can be safely neglected.

The probability of absorbing n photons within the j-th nanowire section is determined by the Poisson distribution:[28,29]

$$P_j^{(n)} = \frac{\mu_j^n \exp(\mu_j)}{n!}, \qquad (4)$$

where μ_j is the number of photons that reach the j-th section of the nanowire. Because of absorption along the waveguide integrated SSPDs, this value varies along the nanowire length as

$$\mu_j = m \exp(-\alpha j w)(1 - \exp(-\alpha w)), \qquad (5)$$

where α is the absorption coefficient of a single strip of the detector and w is the width of the nanowire. The absorption coefficient of the SSPDs is mainly determined by the overlap between the optical field propagating along the waveguide and the nanowires.[21] In our analysis, we extract α by assuming internal quantum efficiency of unity at the maximum bias current ($0.9\,I_c$).

The probability of not absorbing photons in the other sections can then be analogously defined as

$$\Xi_j^{(n)} = \prod_{k=0, k \neq j}^{\mathcal{L}/w} (1 - P_k^{(n)}). \qquad (6)$$

Based on this model, we identify different detection regimes in the measured DP. The fitted results for the different nanowires are shown in Fig. 3. The wider nanowires show three different detection regimes. At high bias current,
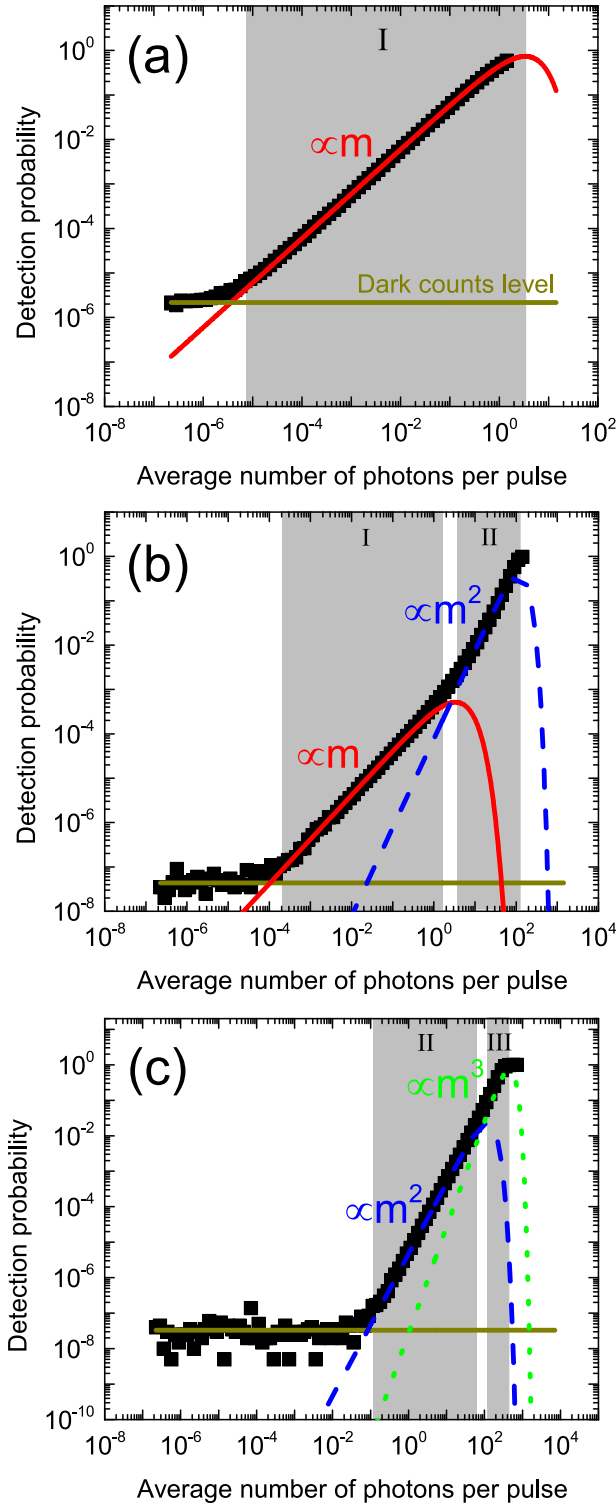

FIG. 3. Fit result of the detection probability curve at different bias conditions for a 120 nm wide nanowire: (a) $I_b = 0.9I_c$, (b) $I_b = 0.5I_c$, and (c) $I_b = 0.4I_c$. The black squares represent the measured data. The detection probability fit for the single photon regime is indicated in red (solid line), the two photon regime in blue (dashed line), and the three photon regime in green (dotted line). The horizontal line (brown) represents the noise level, i.e., the dark count level. The gray shaded areas represented the photon flux regimes where pure one, two, and three photon detection is feasible.

the single photon detection regime is predominant. However, when applying a current lower than $0.5\,I_c$, multi-photon detection is enhanced. Shown in grey are the pure single, double, or triple photon detection regimes. By definition, a pure detection regime occurs when a particular detection mechanism dominates over the others by 3 dB or more.[26] We note, however, that for a number of photons less than one photon per pulse on average, the one photon detection regime is always predominant. When increasing the number of photons per pulse, the multi-photon regime dominates instead. Furthermore, from the measured data for the dark counts (noise) level (brown line in Fig. 3), we observe that the incoming photon number has to be increased at low bias current in order to register a real signal. This is partially due to an overall device sensitivity reduction at lower currents. In addition, the simultaneous presence of multiple photons rapidly declines with decreasing optical input powers which, in turn, reduces the detection probability.

The model proposed above is further used also to determine the *IQE* within the different detection regimes of the SSPDs. In Fig. 4, we show the variation of the *IQE* in dependence of the applied bias current for different detection regimes in a 120 nm wide nanowire and, for comparison, in a 100 nm and an 80 nm wide nanowire. For the 120 nm wide nanowire, the single photon internal quantum efficiency reduces drastically when the bias current is lower than $0.6\,Ic$, where the two photon regime efficiency is enhanced. The same happens again at a bias point of $0.35\,Ic$ between the two and three photon detection regimes. In contrast, for the 80 nm wire, a very low bias current has to be applied to be able to observe the two photon detection regime. In this case, three photon detections cannot be observed. We would also like to point out that the internal quantum efficiency for the single photon detection regime saturates at bias currents in excess of $0.7\,I_c$, which implies that the superconducting detector can be operated at low bias conditions, where dark counts are strongly suppressed and therefore high noise-equivalent power is obtained. The 100 nm wide nanowire shows an intermediate behavior, in which two and three photon detection regimes are visible at very low currents, while the *IQE* saturation occurs at higher bias currents.

In conclusion, we demonstrate that the waveguide integrated superconducting single photon detectors can be designed to work in many photon detection regimes by adjusting the detector width and biasing conditions. A model for the prediction of the detection probability capable of describing the experimental data has been devised. This model also allows for the calculation of the internal quantum efficiency in waveguide integrated SSPDs. The model is in agreement with the QSV theory and shows that wider nanowires are better candidates for simultaneous multiphoton detection. From the internal quantum efficiency calculation, they show in fact a wider bias current range, in which pure two or three photon detection regimes are more efficient than the single photon detection regime. Narrow wires represent an efficient solution for single photon detection. A plateau in the 80 nm and 100 nm nanowires internal quantum efficiency for single photon detection indicates that narrower wires can operate as single photon detectors at lower currents where the signal to noise ratio is very high without any loss in the efficiency.
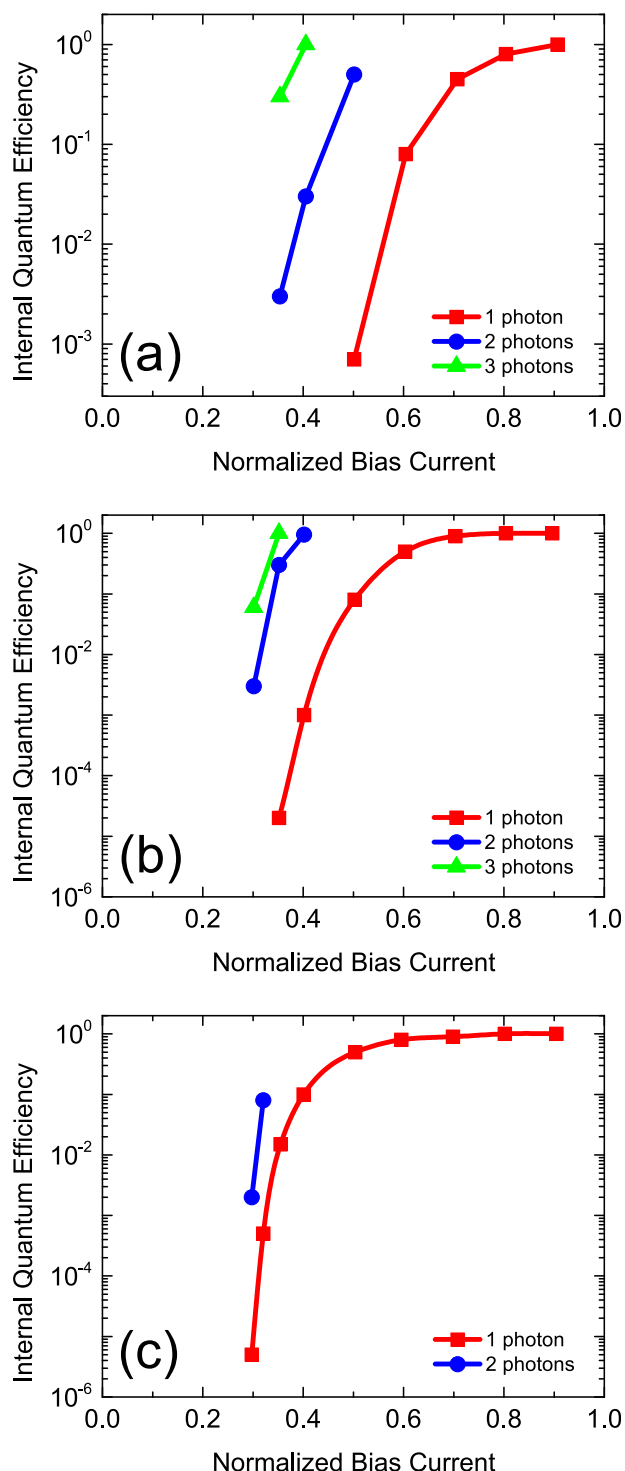
FIG. 4. Calculated internal quantum efficiency for different detection regimes as a function of the bias current, in units of the critical current for (a) 120 nm, (b) 100 nm, and (c) 80 nm wide nanowires.

[1] A. V. Sergienko, Nat. Photonics **2**, 268 (2008).
[2] J. L. O'Brien, Science **318**, 1567 (2007).
[3] J. L. O'Brien, A. Furusawa, and J. Vučković, Nat. Photonics **3**, 687 (2009).
[4] W. Becker, *Advanced Time-Correlated Single Photon Counting Techniques* (Springer, Berlin, Heidelberg, 2005).
[5] H. Dautet, P. Deschamps, B. Dion, A. D. Macgregor, D. Macsween, R. J. McIntyre, C. Trottier, and P. P. Webb, Appl. Opt. **32**, 3894 (1993).
[6] S. Cova, M. Ghioni, A. Lotito, I. Rech, and F. Zappa, J. Mod. Opt. **51**, 1267 (2004).
[7] F. Zappa, Opt. Eng. **35**, 938 (1996).
[8] M. D. Eisaman, J. Fan, A. Migdall, and S. V. Polyakov, Rev. Sci. Instrum. **82**, 071101 (2011).
[9] G. S. Buller and R. J. Collins, Meas. Sci. Technol. **21**, 012002 (2010).
[10] M. A. Itzler, X. Jiang, M. Entwistle, K. Slomkowski, A. Tosi, F. Acerbi, F. Zappa, and S. Cova, J. Mod. Opt. **58**, 174 (2011).
[11] A. Tosi, A. D. Mora, F. Zappa, and S. Cova, J. Mod. Opt. **56**, 299 (2009).
[12] R. H. Hadfield, Nat. Photonics **3**, 696 (2009).
[13] C. M. Natarajan, M. G. Tanner, and R. H. Hadfield, Supercond. Sci. Technol. **25**, 063001 (2012).
[14] C. Schuck, W. H. P. Pernice, and H. X. Tang, Appl. Phys. Lett. **102**, 051101 (2013).
[15] G. N. Gol'tsman, O. Okunev, G. Chulkova, A. Lipatov, A. Semenov, K. Smirnov, B. Voronov, A. Dzardanov, C. Williams, and R. Sobolewski, Appl. Phys. Lett. **79**, 705 (2001).
[16] A. Gaggero, S. J. Nejad, F. Marsili, F. Mattioli, R. Leoni, D. Bitauld, D. Sahin, G. J. Hamhuis, R. Nötzel, R. Sanjines, and A. Fiore, Appl. Phys. Lett. **97**, 151108 (2010).
[17] J. P. Sprengers, A. Gaggero, D. Sahin, S. Jahanmirinejad, G. Frucci, F. Mattioli, R. Leoni, J. Beetz, M. Lermer, M. Kamp, S. Höfling, R. Sanjines, and A. Fiore, Appl. Phys. Lett. **99**, 181110 (2011).
[18] W. H. P. Pernice, C. Schuck, O. Minaeva, M. Li, G. N. Goltsman, A. V. Sergienko, and H. X. Tang, Nat. Commun. **3**, 1325 (2012).
[19] C. Schuck, W. H. P. Pernice, and H. X. Tang, Sci. Rep. **3**, 1893 (2013).
[20] N. Gruhler, C. Benz, H. Jang, J.-H. Ahn, R. Danneau, and W. H. P. Pernice, Opt. Express **21**, 31678 (2013).
[21] V. Kovalyuk, W. Hartmann, O. Kahl, N. Kaurova, A. Korneev, G. Goltsman, and W. H. P. Pernice, Opt. Express **21**, 22683 (2013).
[22] M. G. Tanner, C. M. Natarajan, V. K. Pottapenjara, J. A. O'Connor, R. J. Warburton, R. H. Hadfield, B. Baek, S. Nam, S. N. Dorenbos, E. B. Ureña, T. Zijlstra, T. M. Klapwijk, and V. Zwiller, Appl. Phys. Lett. **96**, 221109 (2010).
[23] L. N. Bulaevskii, M. J. Graf, C. D. Batista, and V. G. Kogan, Phys. Rev. B: Condens. Matter **83**, 144526 (2011).
[24] A. N. Zotova and D. Y. Vodolazov, Phys. Rev. B **85**, 024509 (2012).
[25] R. Lusche, A. Semenov, K. Ilin, M. Siegel, Y. Korneeva, A. Trifonov, A. Korneev, G. Goltsman, D. Vodolazov, and H. W. Hübers, J. Appl. Phys. **116**, 043906 (2014).
[26] M. S. Elezov, A. V. Semenov, P. P. An, M. A. Tarkhov, G. N. Goltsman, A. I. Kardakova, and A. Y. Kazakov, J. Opt. Technol. **80**, 435 (2013).
[27] A. J. Kerman, E. A. Dauler, J. K. W. Yang, K. M. Rosfjord, V. Anant, K. K. Berggren, G. N. Gol'tsman, and B. M. Voronov, Appl. Phys. Lett. **90**, 101110 (2007).
[28] A. D. Semenov, G. N. Gol'tsman, and A. A. Korneev, Phys. C Supercond. **351**, 349 (2001).
[29] B. E. A. Saleh and M. C. Teich, *Fundamentals of Photonics* (John Wiley & Sons, Inc., New York, USA, 1991).